MODELING DRIVE OF PRODUCTION MACHINE ACCORDING TO OUTPUT REQUIREMENTS

RADOMIR PRUSA

Department of Electric Engineering, Faculty of Mechanical Engineering, Brno University of Technology, Brno, Czech Republic

ROSTISLAV HUZLIK

Department of Electric Engineering, Faculty of Mechanical Engineering, Brno University of Technology, Brno, Czech Republic

TOMAS MAREK

Department of Production Machines, Faculty of Mechanical Engineering, Brno University of Technology, Brno, Czech Republic

DOI: 10.17973/MMSJ.2023_10_2023082

Xprusa04@vutbr.cz

The article shows how the drive modelling depending on the required output information, focusing on the machine tool area. In this way, the simulation process can be optimally set up and the output information from the model environment can be used efficiently. From the selection of input parameters to the detail and accuracy of the output values of the model itself. Many authors are dealing with digital twins of production machines. However, they treat the actual drive part of the machine tool as a black box. However, its function occupies a significant part in the creation of such a model. On the other hand, the second part of the authors focus specifically on the actuator modeling, but they do not consider the methodological approach according to the need of output information. This is related to the negative impact on the impracticality of deploying such models in real applications.

KEYWORDS

drive, digital twin, mathematical model, production machine, methodology, SIMULINK

1 INTRODUCTION

The acquisition of experience and scientific knowledge in the field of digital twins is initiated by the growing awareness and demand for the widespread implementation of Industry 4.0 [Reza 2021]. The actual origin is attributed to the NASA (National Aeronautics and Space Administration) space company at the time of the Apollo program [Urban 2019]. The beginning of the mainstream can be placed in the 1990s, when the mass spread of computing occurred. The term digital twin itself was not coined until 2003 at the University of Michigan [Qi 2018]. A generally accepted definition was pronounced in 2012 [Glaessgen 2012]. Other various definitions of a digital twin can be traced, e.g., in [Kroupa 2022]. The digital twin finds application both in the device development phase and in operation to detect and predict system failures. Energy aspects are also part of the models, which can help to reduce and optimize energy consumption e.g. [Ivannikov 2023] [Clausen 2021]. The very concept of digital twins was conceived with the idea of reducing the number of experimental samples required in product development, which is significantly affected by several factors. Subcomponents can be easily subordinated and modified to achieve maximum process efficiency in the shortest possible time. Another use is found in replacing real members of manufacturing systems with virtual ones in such a way that the output characteristics of the whole are not affected. Real-time functionality requires significant computational loop dynamics without additional traffic delays.
Production machines are typically subjected to various compensatory interventions to reduce inherent deviations. The physical action of the external environment on the coupled assembly causes a change in the eigen displacements. If models exist that respect the necessary dependencies, it will be possible to predict the behaviour of real machines.

2 PROBLEM DESCRIPTION

The term drive means the composition of the servomotor and the inverter. A production machine consists of a grouping of several drives that provide different functions. This article deals only with the main drives in the machine that are used to position the workpiece or spindle, i.e., the drives of the individual x, y and z axes. The drive itself is further connected to an external mechanical system. An illustrative diagram is shown in Fig. 1, where the included and considered components of the single axis drive system of the machine tool are shown. The system starts with the control system which feeds the servo motor. The servomotor itself is connected via a flexible coupling to a ball screw providing the conversion of rotary to translation motion. The ball screw is further housed on both sides in a bearing system. The movement of the slider in the ball screw is directed by a linear guide. The axis is also loaded with a possible workpiece or a second axis in the case of a cross table. The position measurement is carried out by means of a rotary and a linear encoder whose signals are fed back to the control system.

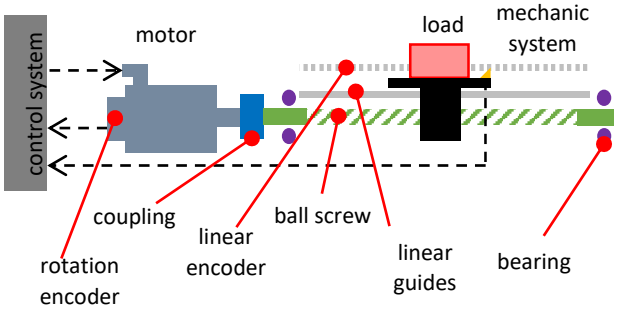

Figure 1. Basic drive conception of one axis in production machine system

Monitoring the positioning accuracy of a machine tool is a highly desirable topic. The aim is of course to achieve the smallest possible positional error from the desired position. Circular interpolation is used as a common tool for monitoring machine tool accuracy. In this case, a circular movement of a specified diameter of the cross table is made relative to the spindle, which forms the centre of the circle. In the described positioning process, the error of the position from the ideal circle of a given diameter is monitored.
The Ballbar diagnostic system is most often used as an evaluation device (see Fig. 2). Its measurement principle is based on the change of the distance between the centre of the circle and the radius of the circle. One point of the measuring system is placed on a fixed point which forms the spindle. The other point is a selected point on the cross table which performs a circular motion. The position error here can arise from a number of causes (see e.g. reference [Vorlicek 1991]), but for the purposes of this paper only the effect from the actuator itself will be investigated. In general, circular motion is problematic for

positioning, as reversal of one of the actuators occurs at the point of axis passage. At these points of reversal, local position distortions occur due to torsional stiffness and finite velocities. The speed of the positioning itself has a significant influence on the magnitude of these peaks.

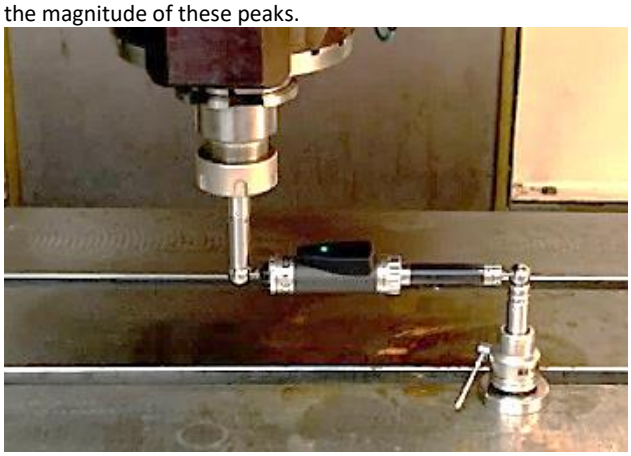

Figure 2. Measurement with Renishaw Ballbar 20

Reversal peaks form a significant positional error, so it is important to address this phenomenon. The tuning of actuators is a very tedious practice, as it is always necessary to verify the new setting by measurement. If a digital twin of the drives of a particular machine tool is deployed, it is possible to achieve a smaller deviation in a short time. Tuning of the drives means setting the control structures in such a way that its dynamics are sufficient and at the same time a minimum deviation is achieved. In the following text, the modelling of the machine tool drive system for the purpose of determining the positional error will be described. This is even with only a marginal knowledge of the overall system. This means that no reassembly of any parts was carried out. All identification was based on external parameter measurements or technical documentation. In order to obtain further necessary information, some values were read directly from the machine tool control system. The control system was also used for some measurements.

3 STATE OF CURRENT KNOWLEDGE

Currently, there are several publications dealing with simulation models of rotating electrical machines that focus on a specific machine type and application (for example [Zhang 2022]). Focusing only on a specific problem, represents a degree of overshadowing for wider use in other applications. A frequent endeavour of many authors is to accurately model a specific machine or part of a machine, this entails an increased load on computational power and the generation of many input parameters (for example [Li 2008]). It is important to decide what needs to be made more accurate for a given application and what does not. A suitable example is the simulation of a magnetic circuit, which can in principle be described in several different ways. In the case of the finite element method (FEM), the nonlinearities of the materials can be affected without much difficulty, on the other hand, it will have a considerable computational time. The same can be achieved by using the electromagnetic analogy and transforming the whole magnetic problem into the form of a discrete magnetic circuit, represented only by sources and magnetic resistors. The resulting time compared to FEM (Finite Element Method) is negligible (for example high accuracy model in [Elsherbiny 2022]).

Drive modelling can currently be divided into a basic pair: mathematical models and FEM-based models (see Fig. 3). Both variants are represented by a system of mathematical equations, the difference is found in their structure. Mathematical models are composed of equations derived from elementary physical equations based on the nature of the machine itself or a specific part. The number of equations is not indicative of the accuracy of the model. On the contrary, the equations of the FEM model describe a specific point of the computational grid, the number of which depends on the desired level of accuracy in the calculation. The basic two groups can be further divided into static, transient and harmonic. The harmonic group can be interpreted as a special case of static models, since it is a steady state process, with periodic variation according to a sine or cosine function [Hrebicek 2006]. Another group of so-called reluctance networks, belonging to the mathematical models, are based on the magnetoelectric analogy and include static and dynamic models of the magnetic circuit [Lovelace 2002]. When a pair of basic models cooperate with each other, a third basic group can be considered (co-simulation). All other models are always based on these categories.

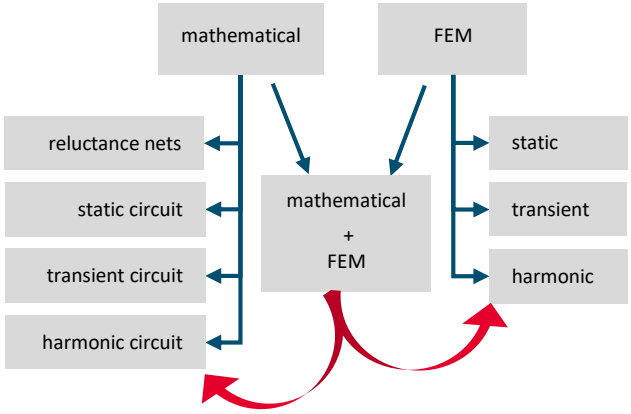

Figure 3. Classification of current drive models

The modelling of the drive in relation to the machine tool is also the focus of some authors. Most of the papers are focused on improving positioning accuracy [Sun 2022] or on optimization methods for control circuit design, such as [Halamka 2021]. Some authors take the route of using Matlab Simulink with the use of extension toolboxes [Pandilov 2015]. It is not the intention in this post to use extension blocks from the Simulink Toolbox. The main reason for this approach is the inability to customize the Toolbox blocks to your needs. Another disadvantage of Toolbox blocks is the license that is required to use them. Licenses for all Matlab Simulink Toolboxes, such as Simscape (suitable for modelling electromagnetic processes), are available by default at Brno University of Technology. Using Simulink basic blocks, a simulation model of the spindle is created in [Malarev 2018]. However, the model lacks any consideration of temperature or current loads in the form of, for example, inductance changes due to magnetic circuit saturation.

The general machine theory is used in [Pillay 1989] to simulate a brushless DC motor drive. The behavior of the controllers in transient states is slated in the paper. In [Spencer 2017] a design method for tuning controllers for high-speed drives is presented in order to achieve the smallest possible positional error. However, the aforementioned paper does not address how signal discretization and quantization factor into the control itself. This fact is very important as these parasitic effects significantly affect the stability of the whole control system.

In addition to drive models, articles dealing with the way of modelling the machining part of the machine tool axis drive can also be found. For example, [Altintas 2011] addresses the ways of implemeting the mechnical model depending on the motion axis components used. A methodological approach to modeling

in terms of the overall energy consumption of a production machine is presented in [Liu 2014].
Last but not least, there is also a sector of cells with predictive control. The authors in [Stephens 2013] tried to implement predictive control in an industrial five-axis CNC (Computer Numerical Control) milling machine.

4 MEASUREMENT

For the purpose of comparison with simulation, validation measurements were carried out on the milling machine form company KOVOSVIT MAS type MCV 754 Quick located at the Institute of production machines, systems and robotics of the Brno University of Technology (see Fig. 4). Where MCV stands for Machining Center Vertical.

Figure 4. KOVOSVIT MAS type MCV 754 Quick on the institute of production machines, systems and robotics

The measurements were made using the diagnostic equipment mentioned above (Ballbar see Fig. 2). The feed rate was selected with respect to the normal machining speed of 1 m/min and 2,5 m/min. The diameter of the circular interpolation was 150 mm. For the evaluation of the measured data the software "Renishaw Ballbar 20" was used. The resulting evaluation for a feed rate of 2.5 m/min is shown in Fig. 5. The quadrant transitions show peaks caused by the actuators. Here the resulting magnitude ranges from 1.5 µm to 3.7 µm. In the case of the 1 m/min velocity, the error due to lower dynamics was smaller. All measurement results including the definition of the conditions are recorded in Tab. 3.
In addition to the conditions of the actual circular interpolation, input parameters for the mathematical model of the drive were of course necessary. In order to obtain these parameters, it was first necessary to analyse which parts the drive in the MCV machine consists of (basic arrangement see Fig. 1 a description).

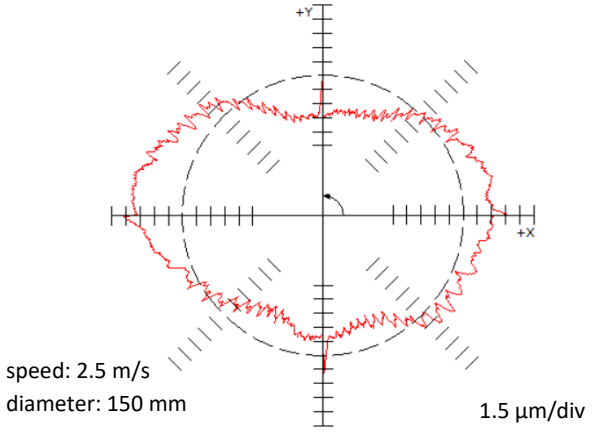

Figure 5. Measurement results of position error on MCV

The built-in servomotor in the MCV machine is type 1FK7080-2AF71-1CG2 from Siemens (see parameters in Tab. 1). The power servo amplifier is also from siemens, specifically type SINAMICS S120 Combi. The couplings used for torque transmission are from KTR, type Rotex GS. The ball screw has a diameter of 32 mm. All the parameters used in the mathematical model of the actuator are shown in Tab. 4. During the execution of the test, there was no significant temperature change due to the low dynamics of the motion. Therefore, simulation model do not include thermal model because measurement was carried out at the initial ambient temperature.

R	0.98	Ω	**2p**	8	poles
L	17.2	mH	**J**	14.2	kg·mm^2
K_T	1.61	Nm/A	**n_{max}**	6000	RPM
I_{max}	18.0	A			

Table 1. Parameters of motor 1FK7080-2AF71-1CG2 [Siemens 2020]

5 IDENTIFICATION PARAMETERS FOR MODEL

The number of input parameters depends on the including of the model dependencies that the model accounts for. The basic information includes motor parameters that are easily traceable in the catalogue: number of poles, winding resistance, inductance, torque constant and motor moment of inertia (see Tab. 1). The motors in both axes are identical, so the parameters are not divided into individual axes.

5.1 Parameters of regulators

From the inverter's point of view, it was necessary to read the gain settings of the inverter control loops from the machine. There were two ways to read the individual parameters from the machine. The first option is to connect the servo amplifier via a communication interface directly via Siemens Starter software to a PC (personal computer). The other option was to read the values directly through the interface implemented in the MCV machine.

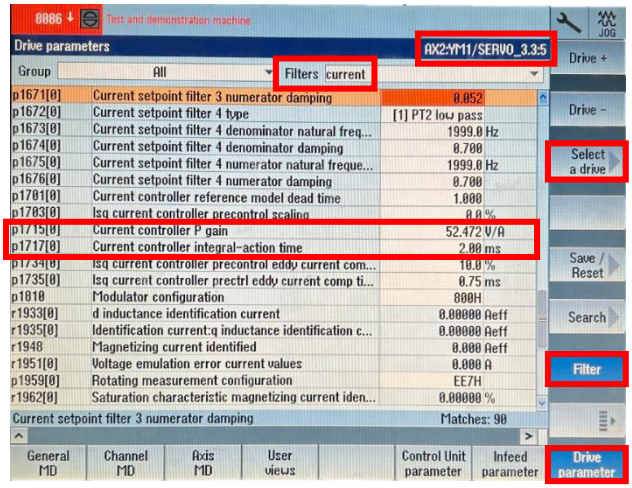

Figure 6. Reading parameters from MCV

Here the second option was used, i.e. using the integrated interface. Fig. 6 shows an example of the display of the current loop gain values in the Y-axis. In order to display the current and speed loop settings, it was necessary to select the "Setup" option in the machine menu via the "MENU SELECT" button. Then select the "Drive parameters" option.
The values of the position controller's so-called speed constant are also stored in "Parameters" under "MENU SELECT". Due to the different moments of inertia, the controllers of each axis are set differently. Specifically, the proportional and integration constants of the current and speed controllers, also the proportional component of the position controller. All numerical values of the mentioned servo amplifier parameters are listed in Tab. 2.

control loops constants		axis X	axis Y
k_{Pi}	V/A	52.472	52.472
k_{Ii}	ms	2.00	2.00
$k_{P\omega}$	Nm·s/rad	8.47	11.67
$k_{I\omega}$	ms	4.05	4.67
k_{Pp}	rad/s/mm	1.7874	1.9686

Table 2. Parameters of control loops in MCV

5.2 *Mechanical parameters*

The content of parameters from the mechanical system is more extensive as it contains more mechanically coupled components than a motor coupled with a dynamometer or a motor without load. Due to the fact that the two axes are different, the parameters are also divided according to the respective axis. Starting from the servomotor, the mechanical system consists of a mechanical coupling, a ball screw, a bearing system, guides and last but not least the carrier for load. This is dependent on the specific axis, as the Y-axis is also loaded by the moment of inertia from the X-axis. In particular, the moment of inertia, which for a ball screw can be calculated according to equation (1), has a significant influence on the dynamic behaviour of the system.

$$J = \frac{1}{2} m \cdot \left(\frac{d}{2}\right)^2 \tag{1}$$

Where d is the diameter of the ball screw and m is the mass determined by length, material density and diameter. In the case of a large ratio of diameter to length, the ball screw also has considerable torsional stiffness, which we also have to calculate and take into account (in this paper is neglected). The mechanical backlash due to the standard tension of the ball screws will be neglected in the model. The couplings stiffness and damping are also catalogue data. Due to the type of couplings, which are referred to as "backlash free", their mechanical backlash will also be neglected.

In addition to the moments of inertia from the rotating parts, there are also moments of inertia due to translational motion mediated by the ball screw. The moment of inertia from the masses performing translational motion is calculated using equation (2).

$$J = m \cdot \left(\frac{s}{2\pi}\right)^2 \tag{2}$$

Where s indicates the pitch of the ball screw.

To identify all the mechanical parameters mentioned, it is necessary to have a good knowledge of the internal arrangement and use of the individual components in the MCV machine. The fact that an disassembled identical cross table is available at the Institute of production machines, systems and robotics was used to advantage and 3D CAD (Three-Dimensional Computer-Aided Design) models were also available (see Fig. 7).

mechanical system			axis X	axis Y
ball screw	pitch	mm/rev	10	10
	inertia	g·m²	0.81	1.28
	stiffness	Nm/rad	528	330
coupling	inertia	g·m²	0.20	0.20
	stiffness	Nm/rad	8335	8335
	damping	-	0.75	0.75
load	inertia	g·m²	0.85	1.36

Table 3. Mechanical parameters (data of coupling [KTR 2023])

All numerical values of the mentioned mechanical parameters are given in Tab. 3.

In this paper, the ball screw bearing model was based on the same principle as bearings for servomotor model (see next chapter about model description). Where the input values of the model are the basic dimensions of the bearings used. Due to the assumed preload of the ball screw, the friction model from chapter 6.4 (external mechanical system) was also used additively, but without the Stribeck effect, which would be complicated the identification of the model parameters.

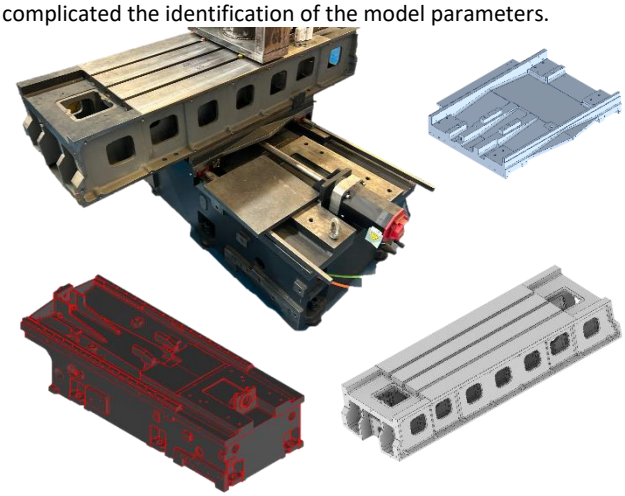

Figure 7. Disassembled and 3D model of cross table

6 MODEL DESCRIPTION

The computational model of a single axis is divided into servomotor, control and mechanical parts (see Fig. 8). A description of each of these parts is given in the relevant subchapters below. When modelling, it was important to keep in mind that the model system must respect the real structure in the machine tool. Matlab Simulink is used for the complete modelling environment.

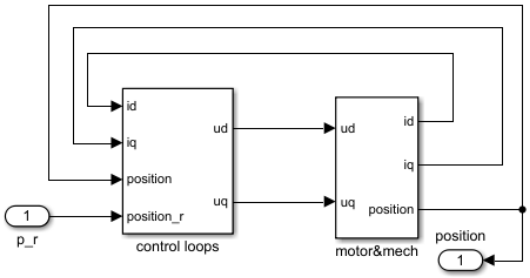

Figure 8. Complete simulation model in Simulink

6.1 Model of synchronous servomotor

In commercial inverters, models of rotating machines in so-called dq coordinates are used for easy control. This model is based on general machine theory [Kron 1951], which can be applied to almost any rotating machine. The basis of this theory is the transformation of the phase coordinates first into αβ coordinates and then into proper dq coordinates.

The differential equations for a general machine given in [Kron 1951] or [Mericka 1973] can be adapted to a form suitable for describing a permanent magnet synchronous machine (3) to (5). Equations (3) and (4) describe the electrical part of the machine. Equation (5) describes mechanical part.

$$\frac{d\Psi_d}{dt} = U_d - Ri_d + \omega_e \Psi_q \tag{3}$$

$$\frac{d\Psi_q}{dt} = U_q - Ri_q - \omega_e(\Psi_d + \Psi_{PM}) \tag{4}$$

$$T_z = \frac{3}{2}\, p\, \Psi_{PM} i_q - J\frac{d\omega_m}{dt} - \beta\omega_m \qquad (5)$$

Where is Ψ magnetic flux, is U voltage, is i current, is t time, is R electric resistance of winding, is p number of poles, is ω angular velocity. Quantities with index "q" belong to the torque production axis and quantities with index "d" to the flux production axis. Quantities with index "e" belong to the electrical and quantities with index "m" are mechanical character. The magnetic fluxes can be expressed by (6),

$$\Psi_d = L \cdot i_d;\ \Psi_q = L \cdot i_q;\ \Psi_{PM} = \frac{\sqrt{2}}{3}\, k_T \cdot p \qquad (6)$$

where L is inductance, k_T is torque constant. Complete dq model is in the Fig. 9.

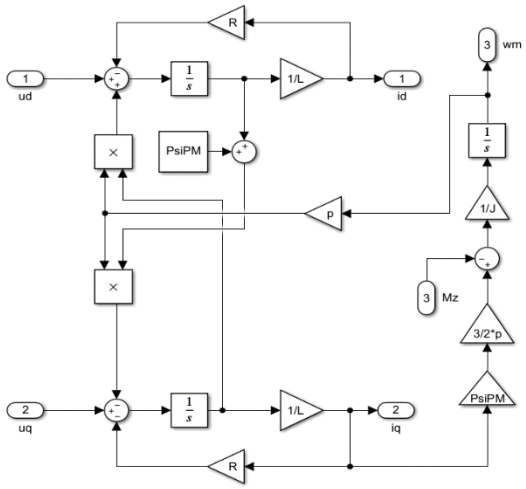

Figure 9. Simulation model of synchronous motor in dq axes

6.2 Control loops

It was necessary to build a control circuit based on the inverter used in the machine tool. Specifically, it is a Siemens S120 Combi inverter, which is handled by the Siemens Starter software.

Control circuits are based on cascade control. In this configuration, one control circuit is linked to another. At the highest position is the position circuit, to which the speed circuit is further subordinated. The lowest level is occupied by the current loop circuit. In the case of a motor model with dq coordinates, it is necessary to control the current in each axis separately, depending on which mode the servomotor is currently in. The output value of the current controller is the desired voltage magnitude in the d and q axes.

In case of servo mode, MTPA (maximum torque per ampere) control is preferred, where the current in the d-axis is held at zero by the controllers and the current in the q-axis is proportional to the magnitude of the shaft torque. Another type of control is the so-called field weakening, which takes place when the nominal point is exceeded. This type of control takes place in such a way that the maximum power of the motor is not exceeded and at the same time the motor speed can be increased. However, during the measurements it was determined that this type of control was not used by the control system, as the axis traverses corresponded to a small speed, e.g. during machining.

The input to each controller is the control error between the desired value and the actual value. It is therefore a feedback control. In total, there are three feedback control circuits. Control in the d and q axis is based on identical gains in both axes according to the Siemens Starter software manual.

Due to the adaptation of the control to the identical control used in the Siemens inverter, it is necessary to respect the internal architecture, which was determined on the basis of the help inside the Starter control software [Siemens 2018]. Position controller use only proportional gain. Current and speed controllers use both proportional and integrating gain. The arrangement between proportional and integration gain can vary from manufacturer to manufacturer (Control Techniques, Kollmorgen, etc.). Siemens used the so-called ideal expression, which is described by equation (7), was used,

$$F(p) = K_P\left(1 + \frac{1}{\tau_I \cdot p}\right) \qquad (7)$$

where $F(p)$ is the image of the Laplace transform, K_P is the amplification constant of the proportional component, rate of the integration component is affected by the integration time constant τ_I. Such an arrangement can also be referred to as a series arrangement. Characteristic of such an arrangement is that the proportional constant also affects the integration gain. The integration gain is defined as the time over which the integration of the deviation takes place. The control system includes current and speed saturation including voltage limitation. All control loops must be defined in discrete mode. Otherwise, the same magnitude of control constants as in the built-in converter could not be used. The entire control could not perform any function without feedback signals, so it is necessary to provide each controller with specific feedback. Feedback signals must also be discrete, as their magnitude is handled by analog-to-digital converters that have a certain sampling time and number of signal levels (see chapter about 6.5). A view of the entire control structure used in the model can be found in Fig. 10.

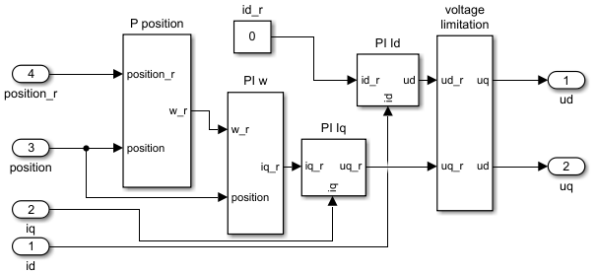

Figure 10. Control loops in model

The units of the control gains correspond to the described system, which are shown in Tab. 1. The aim of this paper is not to show how to achieve the smallest errors, but how to approach the specific purpose of the simulation. Specifically, to obtain positional error information. Therefore, for simplicity, no compensation processes have been introduced into the control systems. For this reason, all compensation processes were also disabled in the machine tool control system when applying individual measurements.

6.3 Mechanical system

The mechanical system is a very important part for respecting the phenomena that arise in a real drive. At first, the focus was on the mechanical phenomena arising in the actual servo motor. Concretely, these are mechanical losses caused by bearings and ventilation losses.

In general, ventilation losses are mainly generated by cooling fan friction. In the case of servomotors, however, this phenomenon is eliminated due to the absence of an internal or external fan. Therefore, it follows from the preceding text that the total ventilation losses will be limited only to those due to frictional losses in the narrow air gap, i.e. the gap between the stator and the rotor. Literature [Pyrhonen 2014] dealing with the overall design of electrical machines contains a calculation procedure for the described problem. The torque from ventilation loss is equal to (8),

$$T_{vent} = \frac{1}{32} \cdot k \cdot C_M \cdot \pi \cdot \rho \cdot \omega_m^2 \cdot D_r^4 \cdot l_r \quad (8)$$

where k is the roughness coefficient, C_M is the moment coefficient according to equation (10), ρ is the density of the internal medium, D_r is the rotor diameter and l_r is the rotor packet length. According to literature [Pyrhonen 2014], the value of the roughness coefficient is chosen in the range of 1÷1.4. Here, due to the existence of permanent magnets on the surface, a value of 1.4 was considered. Furthermore, the determination of the moment coefficient is based on the calculation of the Reynolds number, which is determined on the basis of equation (9),

$$Re_\delta = \frac{\rho \cdot \omega_m \cdot D_r \cdot \delta}{2 \cdot \mu} \quad (9)$$

where δ is the thickness of the air gap and μ is the dynamic viscosity of the internal medium. According to the resulting value, the specific form of the equation for the moment coefficient is then used. Based on the analysis performed, it was determined that the Reynolds number in the air gap does not exceed 64 in the case of servomotors. This corresponds to the equation (10). In the literature [Pyrhonen 2014] other variants of the relationships can be traced for higher values of the Reynolds number.

$$C_M = 10^{\cdot \frac{\left(\frac{2 \cdot \delta}{D_r}\right)^{0,3}}{Re_\delta}} \quad (10)$$

For these calculations it is necessary to know the inner diameter of the rotor and its length. These dimensions can be estimated from the outer dimensions of the servomotor according to equations (11) and (12),

$$D_r = 0{,}57 \cdot w_f \quad (11)$$

$$l_r = 0{,}53 \cdot l_f \quad (12)$$

where w_f is frame width and l_f is frame length. Both equations were determined by measuring the internal structure of several commercial servomotors. The equations are valid for servomotors with 8 and 10 poles because the length of the winding end is approximately the same. This range is based on the observation that the vast majority of servomotors are of this pole count design.

The calculation of the bearing loss moments is based on the model presented by [SKF 2006]. Equation (13) gives the total torque generated by the pair of bearings carrying the servomotor rotor.

$$T_{bearing} = 2 \cdot (M_{rr} + M_{sl} + M_{seal}) \quad (13)$$

Where M_{rr} is the moment of rolling friction, M_{sl} is the moment of shear friction, M_{seal} is the moment from the seal. The calculation and description of the individual components is given in document [SKF 2006]. Furthermore, the resulting relationship was simplified by neglecting the torque caused by the wading of bearings in oil, since servomotors use mostly sealed bearings with solid lubricant.

As in the case of the ventilation calculation, it is necessary to estimate the bearings used. It is necessary to reveal the first probable bearing size and assume the same size on both sides of the rotor. Alternatively, an order of magnitude larger bearing can be considered on the shaft side than on the non-shaft side. The bearing size estimate is based on the diameter of the output shaft and again the outer dimension of the frame.

6.4 External mechanical system

The external mechanical system is based on the same bearing model as inside the servomotor. This model can be used, for example, to house ball screws. However, it is also necessary to consider the friction caused by the guidance and function of the ball screw. Due to the preloading of the ball screws to prevent backlash, it is necessary to include its torque too. The friction model used within this paper includes. Due to the preload and the use of no-backlash couplings, backlash can be neglected.

Four types of friction can occur during motion, i.e. static, Coulomb friction, Stribeck effect and viscous dynamic friction [Palkovic 2012]. Due to the difficulty of determining the Stribeck effect, a model representing only Coulomb and viscous friction was used. The resulting sum of two friction components gives rise to a characteristic (see Fig. 11), which is described by equation (14).

$$T_{friction} = M_v \cdot \omega_m + M_c \cdot sgn(\omega_m) \quad (14)$$

where M_v is the moment coefficient of viscous dynamic friction, M_c is the moment coefficient from Coulomb friction.

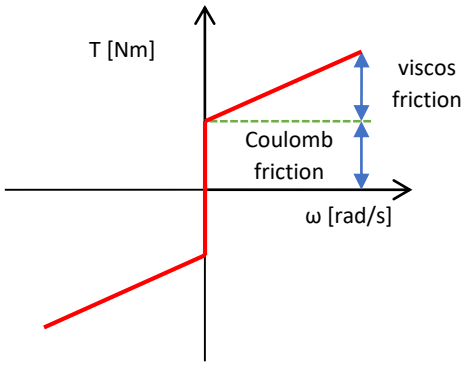

Figure 11. Friction model for external mechanical system (figure was taken from [Palkovic 2012] and edited)

Furthermore, due to the use of couplings between the motor and the ball screw, it is necessary to also include torsional stiffness model according to equation (15),

$$\frac{d\varphi}{dt^2} = \frac{1}{J}\left(T - b \cdot \frac{d\varphi}{dt} - k \cdot \varphi\right) \quad (15)$$

where J is the moment of inertia, φ is the angle of rotation in time and b is the damping coefficient.

In the case of rotary couplings, the amount of damping is usually given in the form of the relative attenuation ξ. This can be converted into a damping coefficient according to the actual shaft speed using relation (16),

$$b = \frac{k \cdot \xi}{2\pi \cdot \kappa \cdot \omega} \quad (16)$$

where κ is the order of the harmonic component.

6.5 Other optional model properities for positioning

The process of positioning error is also sensitive to the included parasitic properties that affect the process within the regulatory structures. For this reason, the following list of parasitic properties were included in the model:

Sampling and quantization speed

Due to the rotor encoder, it is necessary to perform the discretization and quantization on a specific rotor rotation and then calculate a specific speed. The size of the quantitation unit q_u is determined using the equation (17),

$$q_u = \frac{2\pi}{2^{n_{tb}}} \quad (17)$$

where n_{tb} is number of transducer bits.

Sampling and quantization measure current

Similarly, to the speed feedback, discretization and quantization of the current signal was implemented. The quantization unit q_u

is given by the range of the current sensor and the number of transducer levels, see equation (18).

$$q_u = \frac{I_{csr}}{n_{tl}} \tag{18}$$

where I_{csr} is current sensor range and n_{tl} is number of transducer levels.

Noise in current sensor

According to [Lazar 2019], noise in electric drives is caused by harmonic and interharmonic components. The spectral density of noise in electric drives was dealed also for example in [Ioannis 2014]. For the purposes of the model, it would be impractical to determine the individual components, so it is more appropriate to represent the entire spectral region. In addition, other interfering elements enter the system. For simulation general noise with neglected significant components such as the inverter carrier frequency, was choose a "white noise" block for use. Advantage of this block has constant spectral density, i.e. the spectral power is the same for the same width in any frequency band. It is defined in units of spectral power, i.e., watts per hertz (W/Hz). The reason for using noise is to expose the control system to sudden superimposed changes in the main signal, for this reason it is best to use white noise as it contains the entire frequency band. The sampling period shall be chosen to be significantly less than the smallest time constant of the system according to equation (19).

$$sampling\ period \approx \frac{1}{100 \cdot f_{max}} \tag{19}$$

In the case of an electric drive, f_{max} shall be determined by equation (20), where n is the number of revolutions per minute.

$$f_{max} = p \cdot \frac{n}{60} \tag{20}$$

Inverter switching frequency

From the control point of view, the switching frequency of the inverter itself is important. Because each control action can be carried out in the worst case only in one period. In the second limiting case, it can be executed immediately at the time of the request for control intervention. In general, this is the interval defined by the two time stamps. In terms of probability, specifically considering a Gaussian normal distribution, the highest probability falls on a regulatory intervention time equal to half a period. The described time period causes the so-called inverter transport delay, which can be determined by equation (21), where f_{VM} is switching frequency of inverter.

$$T_{dVM} = \frac{1}{2} \cdot \frac{1}{f_{VM}} \tag{21}$$

6.6 Model of cross table

The block diagram of the modified model for the two-axis application is shown in Fig. 12. These position signals continue to the models representing the X and Y position axis of the cross table. The output of each model is the actual position in that axis. However, both input and output data are in the Cartesian coordinate system. For proper evaluation, this positional data must be converted to the polar coordinate system. The coordinate transformation is performed via equations (22) and (23).

Equation (22) gives the radius r and equation (23) gives the position angle φ at which the radius is located. The input values are positional data in the Cartesian coordinate system x and y. The equation for calculating the angle is based on the cyclometric tangent function, which, if implemented directly in the model without further programming treatment, would not perform the expected function correctly. Because it has only one input information, which is the ratio of the two coordinates and thus cannot respect the individual quadrants of the polar coordinates. It is therefore possible to use a modified function in most software, which is often referred to as "arctg2(x,y)". This function contains a separate port for both coordinates. The function described is also part of the standard blocks in Matlab Simulink. The output of this block is defined by the range - π ÷ π so it is necessary to additionally implement the derivation from the negative position of the x-axis summing with 2π after the angle π is exceeded.

$$r = \sqrt{x^2 + y^2} \tag{22}$$

$$\varphi = arctg\left(\frac{y}{x}\right) \rightarrow arctg2(x, y) \tag{23}$$

In the polar coordinate block, the error from the desired position is calculated, and this error is then converted to polar coordinates according to the transformation described above for subsequent creation of the circle diagram. The model thus created had to be further supplemented with input parameters. The parameters for the model generating the load moment from the bearing arrangement were obtained in according to text about mechanical system. The ball screw is also housed in a bearing system consisting of one pair of bearings. Their size was determined in the process of determining the mechanical parameters of the cross table.

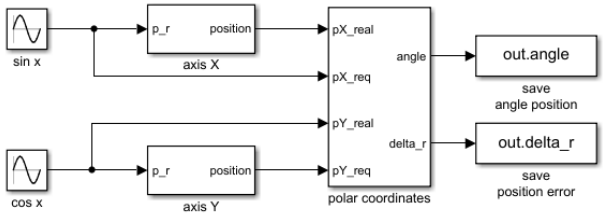

Figure 12. Simulation model for circular interpolation in Simulink

7 VERIFICATION SIMULATIONS

Before simulating the circular interpolation, additional test measurements were performed to investigate the behaviour of the controllers within each axis. The actual measurement was based on a positional transition from the 0 mm initial position to the 200 mm position in both axes. The control structures in the machine tool are set to the values shown in the Tab. 2 by default. Therefore, the same values will be considered for the purpose of the next simulations on MCV milling machine.

Due to the preload of the ball screws and the friction in the linear axis guides, it is not sufficient to use a loss model based on rolling bearings only. Therefore, traversing measurements were also used to identify these additional frictional losses. The crossing speeds were chosen to be close to the measurements when performing the circular interpolation. The identification of the losses was based on speed and current measurements and electrical power input. As a result of the identification, a lookup table of friction according to the actual speed was obtained, which was simultaneously correlated with the loss model in the bearing system.

For illustrative purposes, a crossing speed of 5 m per minute was selected to show the results of the comparison between simulated and measured current, this is shown in Fig. 13 and Fig. 14. The quantity compared was the value of the q-axis current, which is proportional to the magnitude of the output torque on the shaft according to the moment constant. From the obtained waveforms, it can be seen that the Y-axis has a higher moment of inertia which will cause a higher peak current.

Further, the steady state current value shows a higher value than the X axis as it also has a higher frictional resistance. The deviation between the measurement and simulation can be seen by looking at the peak currents that deviate. This may be due to not including the change in inductance as a function of the flowing current.

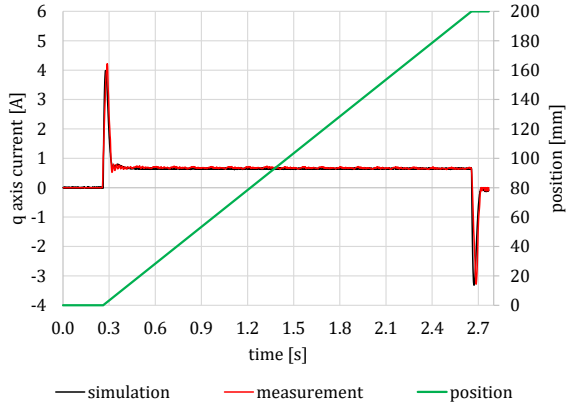

Figure 13. Trapezoidal trajectory in X axis – q current

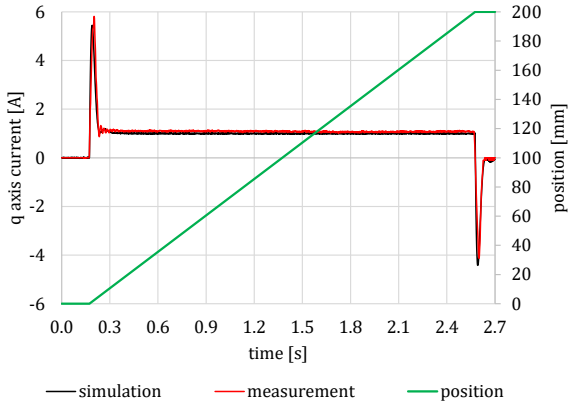

Figure 14. Trapezoidal trajectory in Y axis – q current

8 SIMULATON OF CIRCULAR INTERPOLATION

After performing the described control and identification measurements, we proceeded to the actual simulation of the circular interpolation. Based on these parameters and the presented modelling method, the simulation of circular interpolation was performed for three positioning speeds and a circle diameter of 150 mm.

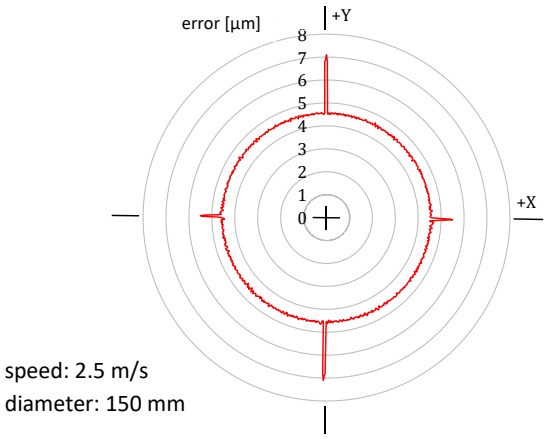

Figure 15. Simulation of circular interpolation with speed 2.5 m/s

The resulting positional error for a velocity of 2.5 m/s was plotted in a polar plot, which is shown in Fig. 15. The resulting deviation diagram shows a steady state deviation of about 4.5 µm. Furthermore, a quadrant of reversal peaks that occur in the transitions between quadrants can be seen.

The modelling also investigated the effect of including of quantization and noise. In the case of switching off the noise and the quantization of the current including the quantization of the position, the resulting deviation diagram gets a smooth steady-state waveform (the region between the reversal peaks). However, when comparing the steady-state deviation character of the measured circular interpolation, ripples are also evident, as in the case of the model variant respecting these parasitic properties (see Fig. 5 and Fig. 15). The difference in average steady-state deviation between the models representing the two variants is less than 0.1 µm. In the case of transition regions, noise and quatization are manifested in the asymmetry of the reservation peaks (in same axis). This is again consistent with the measured deviation diagram, which does not have symmetric reversion peaks within the axes. The caused symmetry difference was also below 0.1 µm.

position error of reversal spikes [µm]	speed [m/s]		
	0.3	1.0	2.5
measure ±X	0.2 / 0.3	1.0 / 0.5	1.5 / 1.5
simulation ±X	0.1	0.7	1.2
measure ±Y	0.9 / 0.9	2.2 / 2.1	2.9 / 3.0
simulation ±Y	0.5	1.4	2.5

Table 4. Circular interpolation - measurement a simulation

When comparing the results obtained, it is necessary to consider the measure tolerance of the Ballbar system used, which is given as 1.25 µm (20 °C). The accuracy of the sensor itself is 0.50 µm (20 °C) [Renishaw 2010]. Consequently, this creates a tolerance band where the measurand can be located.

For the same positioning speed, the deviation diagram obtained from the MCV measurements using Ballbar was shown in Fig. 5. When compared, it is clear that the deviation diagram shows a different shape in the steady-state deviation section. This deformation is due to influences that are not part of the investigation of this paper. According to the shape of the resulting deformation, it is possible to determine what causes the circular inaccuracy based on relevant knowledge. As a rule, it may be an imperfection of the right angle between the cross table and the spindle. In case of a deeper interest in the subject, it is possible to find these reasons in the relevant literature dealing with the subject, such as [Vorlicek 1991].

Therefore, further comparisons between simulated and measured deviations must be approached only in terms of the resulting magnitudes. Which, in the case of focusing on the steady state deviation just discussed, is a value similar to that of the simulation, i.e. 4.5 µm. Furthermore, from the viewpoint of the reversal peaks, it can be seen that higher values of deviation occur in the Y-axis than in the X-axis. This fact is also consistent with the measured diagram. The difference in each axis is due to the different mass of the moving components and hence the moment of inertia. To some extent, this effect should be compensated by the different settings of the controllers. However, the parameters are probably tuned for a cross table loaded with a workpiece of a certain weight. The size of the reversal peak in the Y-axis reaches 2.6 µm in the case of the simulation and measured in the range of 3.5÷3.7 µm. In the case of the X-axis, the absolute difference between simulated and measured deviation is similar (simulated 0.9 µm and measured range 1.5÷1.6 µm).

The next simulation results of position errors of reversal spikes for velocities of 0.3 and 1.0 m/s are shown in Tab. 4 together

with the values obtained from the measurements for comparison. Furthermore, in terms of again the absolute difference between simulated and measured, the values are similar across all velocities. The difference may be in the way of some neglected properties or a difference in frictional moments. In any case, this described difference may be the subject of further research.

9 APLICATION OF THE MODEL

In a first approximation, the control structure of the machine tool can be tuned without the need for a physical machine thanks to deviation monitoring. In case of adding a temperature model, it will be possible to monitor how the servomotor parameters change during the process and adjust and tune the control system accordingly. The topic of the temperature model is continued in observing the warming of individual drives during the execution of the working cycle thanks to the developed problem. On the basis of this, the compensation map can be modified to take into account the warming of the individual drives in certain areas of the machine tool. Of course, this can also be done on the basis of measurements, but it may be the case that the machine is not yet available, i.e. it is, for example, in the development phase. At this stage, the use of models (digital twins) is particularly advantageous as it is possible to adapt the design of the entire machine during the design phase. A further benefit can be the energy consumption of the entire designed machine, where the total energy consumption can be predicted on the basis of known duty cycles. Last but not least, the problem of tuning the drives of a new machine also arises, if at least basic information is available, it is possible to set most of the drives before the actual production. In a second approximation, it is possible to also observe the dependence of positioning accuracy on changes in the internal structure of the servo motor. This includes changes in the winding parameters, the state of the permanent magnets or the magnetic circuit. If these changes are respected and then implemented in the change of the individual control structures, it is possible to achieve an increase in accuracy from a different perspective.

10 CONCLUSIONS

The collective tendency to take current technological advances higher initiates the possibilities of widespread digitisation. This direction is also firmly linked to the actual computational models that must be optimally used and integrated for these purposes.
The starting point for the actual development of the methodology was the model in the so-called dq coordinates. Among the key reasons for the choice of modelling was the use of this type in the commercial sphere.
The control system is also important, as it determines the behaviour of the servomotor itself under dynamic or static loading. Given the fact that servo motors from different companies contain different internal structures, it was important to address this issue as well.
During operation, many parasitic properties affect the operation or measurement of quantities. Noise, inverter switching frequency, discretization and quantization of the measured signal were selected as suitable important parasitic properties. Along with electrical parasitic properties, mechanical friction, torsional stiffness are also included. In the absence of input parameters, the model cannot perform its function as a digital twin, so the identification of these electrical and mechanical parameters was included.
By comparing the measured and simulated characteristics, whether positional or current, it was verified that the above modelling methodology can be used to simulate the positional errors of machine tool axes.

ACKNOWLEDGMENTS

This work is an output of BUT research project Reg. No. FSI-S-23-8260 - Chytre vyrobni systemy (Smart production systems).

REFERENCES

[Altintas 2011] Altintas, Y. and Verl, A. Machine tool feed drives [online]. 2011, No2., [23-5-2023]. Available from <https://www.sciencedirect.com/science/article/pii/S0007850611002125>. 10.1016/j.cirp.2011.05.010.

[Clausen 2021] Clausen, A. and Arendt, K. A digital twin framework for improving energy efficiency and occupant comfort in public and commercial buildings [online]. Sep 2021, No.40, revision [2023-5-16]. Available from < https://doi.org/10.1186/s42162-021-00153-9>.

[Elsherbiny 2022] Elsherbiny, H. and Szamel, L. High Accuracy Modeling of Permanent Magnet Synchronous Motors Using Finite Element Analysis [online]. Oct 2022 [23-5-2023]. Available from <https://www.mdpi.com/2227-7390/10/20/3880>. DOI: 10.3390/math10203880.

[Glaessgen 2012] Glaessgen, and Stargel, D. The Digital Twin Paradigm for Future NASA and U.S. Air Force Vehicles [online]. 2012, No.53, Structures, Structural Dynamics, and Materials Conference: Special Session on the Digital Twin [2023-5-16]. https://ntrs.nasa.gov/api/citations/20120008178/downloads/20120008178.pdf

[Halamka 2021] Halamka, V. and Moravec, J. Drive axis controller optimization of production machines based on dynamic models [online]. July 2021, [23-5-2023]. Available from <https://rcmt.cvut.cz/wp-content/uploads/2022/01/2021_Moravec-Koubek_DMSVZ1.pdf>. DOI: 10.1007/s00170-021-07160-w.

[Hrebicek 2006] Hrebicek, J. and Skrdla, M. Uvod do matematickeho modelovani. Identification code. Masaryk University, 2006.

[Ioannis 2014] Ioannis, T. and Tischmacher, H. Influence of the Inventers's Modulation Technique on the Audible of Electric Motors [online]. Jan 22014 [23.5.2023]. Available from <https://ieeexplore.ieee.org/document/6530675>. DOI: 10.1109/TIA.2013.2268453.

[Ivannikov 2023] Ivannikov, M. Digital Twins: A Key to Energy Saving in Manufacturing. Automation.com, 2023, l [online]. [2023-5-16]. Available from <https://www.automation.com/en-us/articles/march-2023/digital-twins-key-energy-saving-manufacturing>.

[Kron 1951] Kron, G. Synchronous machine reference frames. Electrical Engineer (online), 1951 [23.5.2023]. Available from < http://ieeexplore.ieee.org/document/6436710/>, DOI: 10.1109/EE.1951.6436710.

[Kroupa 2022] Kroupa, J. Navrh digitalniho dvojcete obrabeciho stroje. Brno University of Technology, 2022.

[KTR 2023] KTR, Bezvůlové servospojky ROTEX GS. 2023, Available from < https://www.ktr.com/fileadmin/ktr/media/Tools_Downloads/kataloge/DriveTechnology.pdf >.

[Lazar 2019] Lazar, R. The use of Model Predictive Control (MPC) in motor drives for switching loss and motor noise reduction [online]. Nov 2019 [23.5.2023]. Available

from <https://ieeexplore.ieee.org/document/8915543>. DOI: 10.23919/EPE.2019.8915543.

[Li 2008] Li, Z. and Zhu, J. Comparison of alternate analytical models for predicting cogging torque in surface-mounted permanent magnet machines [online]. 2008 [23.5.2023]. Available from < https://ieeexplore.ieee.org/document/4677557>.DOI:10.1109/VPPC.2008.4677557.

[Liu 2014] Liu, F. and Xue, J. A method for predicting the energy consumption of the main driving system of a machine tool in a machining process [online]. Sep 2014 [23-5-2023]. Available from <https://www.sciencedirect.com/science/article/pii/S0959652614009883>. DOI: 10.1016/j.jclepro.2014.09.058.

[Lovelace 2002] Lovelace, C. and Jahns, M. A saturating lumped-parameter model for an interior PM synchronous machine. [online]. 2002, No.38, [2023-5-16]. Available from < http://ieeexplore.ieee.org/document/1003413/>. DOI: 10.1109/TIA.2002.1003413. ISSN 0093-9994.

[Malarev 2018] Malarev, V. and Kopteva, A. Electric Drive Simulation for Drilling Machine Spinner [online]. 2018, [23-5-2023]. Available from <https://iopscience.iop.org/article/10.1088/1755-1315/194/5/052012/pdf>. DOI 10.1088/1755-1315/194/5/052012.

[Mericka 1973] Mericka, J. and Zoubek, Z. General theory of electric machine. Praha, 1973.

[Palkovic 2012] Palkovic, M. and Makys, P. Influence of static friction and stick-slip phenomena on control quality of SMPM [online]. June 2012. Available from < https://ieeexplore.ieee.org/stamp/stamp.jsp?tp=&arnumber=6225644>.

[Pandilov 2015] Pandilov, Z. and Milecki, A. Virtual modelling and simulation of a CNC machine feed drive system [online]. 2015, [23-5-2023]. Available from < https://www.researchgate.net/publication/298046347_Virtual_modelling_and_simulation_of_a_CNC_machine_feed_drive_system>.

[Pillay 1989] Pillay, P. and Krishnan, R. Modeling, Simulation, and Analysis of Pemanent-Magnet Motor Drives, Part II: The Brudhless DC Motor Drive [online]. March 1989, [23-5-2023]. Available from <https://ieeexplore.ieee.org/abstract/document/25542>. DOI: 10.1109/28.25542.

[Pyrhonen 2014] Pyrhonen, J. and Jokinen, T. Design of rotating electrical machines. 2nd ed. Chichester. Wiley, 2014. ISBN 978-1-118-58157-5.

[Qi 2018] Qi, Q. and Tao, F. Digital Twin Service towards Smart Manufacturing [online]. 2018, pp 237-242, 72, [2023-05-16]. Available from < https://linkinghub.elsevier.com/retrieve/pii/S2212827118302580>. ISSN 22128271.

[Renishaw 2010] Renishaw, Diagnosticky system Ballbar QC20-W – popis a specifikace. 2010, Available from < https://www.renishaw.cz/media/pdf/cs/fe351a817c58463cad0c9047cfe9143c.pdf>.

[Reza 2021] Reza, M. and Malarvizhi, Ch. Industry 4.0–Technological Revolution and Sustainable Firm Performance [online]. May 2021, [2023-5-16]. Available from <https://ieeexplore.ieee.org/stamp/stamp.jsp?tp=&arnumber=9619363>. ISBN:978-1-6654-2237-6.

[Siemens 2018] Siemens, SINAMICS S120 Starter drive functions, Available from < https://cache.industry.siemens.com/dl/files/573/109757573/att_961363/v1/S120_drive_fct_man_0718_en-US.pdf>.

[Siemens 2020] Siemens, Data sheet for SIMOTICS S-1FK7. 2020, Available from <https://mall.industry.siemens.com/mall/en/WW/Catalog/Product/1FK70802AF71-1CG2>.

[SKF 2006] SKF: The SKF model for calculating the frictional moment. 2006. Available from https://www.skf.com/binaries/pub12/Images/0901d1968065e9e7-The-SKF-model-for-calculating-the-frictional-moment_tcm_12-299767.pdf.

[Stephens 2013] Stephens, A.M. and Manzie, Ch. Model Predictive Control for Reference Tracking on an Industrial Machine Tool Servo Drive [online]. May 2013 [23-5-2023]. Available from <https://ieeexplore.ieee.org/stamp/stamp.jsp?tp=&arnumber=6327360>. DOI: 10.1109/TII.2012.2223222.

[Sun 2022] Sun, X. and Cai, F. Finite Position Control of Interior Permanent Magnet Synchronous Motors at Low Speed, Jan 2022 [23.5.2023]. Available from <https://ieeexplore.ieee.org/abstract/document/9695366>. DOI: 10.1109/TPEL.2022.3146841.

[Urban 2019] Urban, P. Digitalni dvojce: Technologie NASA miri do podnikovych informacnich systemu, 2019, [online]. [2023-05-16]. Available from < https://www.systemonline.cz/it-pro-logistiku/digitalni-dvojce.htm >.

[Vorlicek 1991] Vorlicek, Z. Splehlivost a diagnostika vyrobnich stroju: Czech University of Technology, 1991. ISBN 80-010-0510-0

[Zhang 2022] Zhang, X. and Wang, Z. Anti-Disturbance Integrated Position Synchronous Control of a Dual Permanent Magnet Synchronous Motor System [online]. Sep 2022 [23.5.2023]. Available from <https://www.mdpi.com/1996-1073/15/18/6697>. DOI: 10.3390/en15186697.

CONTACTS:

Ing. Radomir Prusa
Brno University of Technology, Faculty of Mechanical Engineering, Department of Electrical Engineering
Address, Brno, 616 69, Czech Republic, +420 541 142 106, xprusa04@vutbr.cz, www.vutbr.cz

Ing. Rostislav Huzlik, Ph.D.
Brno University of Technology, Faculty of Mechanical Engineering, Department of Electrical Engineering
Address, Brno, 616 69, Czech Republic, +420 541 143 419, huzlik@vutbr.cz, www.vutbr.cz

Ing. Tomas Marek, Ph.D.
Brno University of Technology, Faculty of Mechanical Engineering, Department of Production Machines
Address, Brno, 616 69, Czech Republic, +420 541 142 451, Tomas.Marek@vut.cz, www.vutbr.cz